JACS
JOURNAL OF THE AMERICAN CHEMICAL SOCIETY
Communication
Cite This: J. Am. Chem. Soc. 2017, 139, 14352-14355
pubs.acs.org/JACS

Pomeranz–Fritsch Synthesis of Isoquinoline: Gas-Phase Collisional Activation Opens Additional Reaction Pathways

Shibdas Banerjee,[#,†,∥] Fang Liu,[#,†,§,‡] David M. Sanchez,[†,§,‡] Todd J. Martínez,[†,§,‡] and Richard N. Zare[*,†]

[†]Department of Chemistry and [§]The PULSE Institute, Stanford University, Stanford, California 94305, United States
[‡]SLAC National Accelerator Laboratory, Menlo Park, California 94025, United States
[∥]Indian Institute of Science Education and Research Tirupati, Tirupati 517507, India

Supporting Information

ABSTRACT: We have investigated the gas-phase production of isoquinoline by performing collisional activation on benzalaminoacetal, the first intermediate in the classic solution-phase Pomeranz–Fritsch synthesis of isoquinoline. We have elucidated the reaction pathways in the gas phase using tandem mass spectrometry. Unlike the corresponding condensed-phase reaction, where catalytic proton exchange between intermediate(s) and solvent (Brønsted–Lowry base) is known to drive the reaction, the gas-phase reaction follows the "mobile proton model" to form the products via a number of intermediates, some the same as in their condensed-phase counterparts. Energy-resolved mass spectrometry, deuterium labeling experiments, and theoretical calculations (B3LYP/6-31G**) identified 27 different reaction routes in the gas phase, forming a complex interlinked reaction network. The experimental measurements and theoretical calculations confirm the proton hopping onto different basic sites of the precursors and intermediates to transform them ultimately into isoquinoline.

The Pomeranz–Fritsch reaction[1] is a popular gateway to the synthesis of isoquinoline derivatives, finding several important applications in the production of pharmaceuticals, dyes, and other fine chemicals. The archetypical reaction used concentrated sulfuric acid as the catalyst to synthesize isoquinoline from benzaldehyde and 2,2-dialkoxyethylamine (Scheme S1). Afterward, many literature precedents showed modification of this synthesis by using varieties of catalysts, substrates, and reaction conditions.[2] Recently, we showed the reaction rate for the Pomeranz–Fritsch reaction to be nearly a million times faster in charged microdroplets when compared to bulk.[3] In all of these cases, the basic underlying mechanism of the reaction remains similar, although different methods are followed. In the solution phase, the synthesis is carried out in two steps: condensation of benzaldehyde and 2,2-dialkoxyethylamine to form the benzalaminoacetal, followed by acid-induced ring closure to yield isoquinoline (Scheme S1).

The present work describes the feature of the Pomeranz–Fritsch reaction, in contrast to the solution-phase reaction, in the gas phase when the protonated benzalaminoacetal (**1** in Figure 1) precursor was collisionally activated, followed by the tandem mass spectrometric (MS) interrogation of the gaseous intermediates and product. In the tandem MS experiment (Figure S2), the precursor species is ionized and introduced to

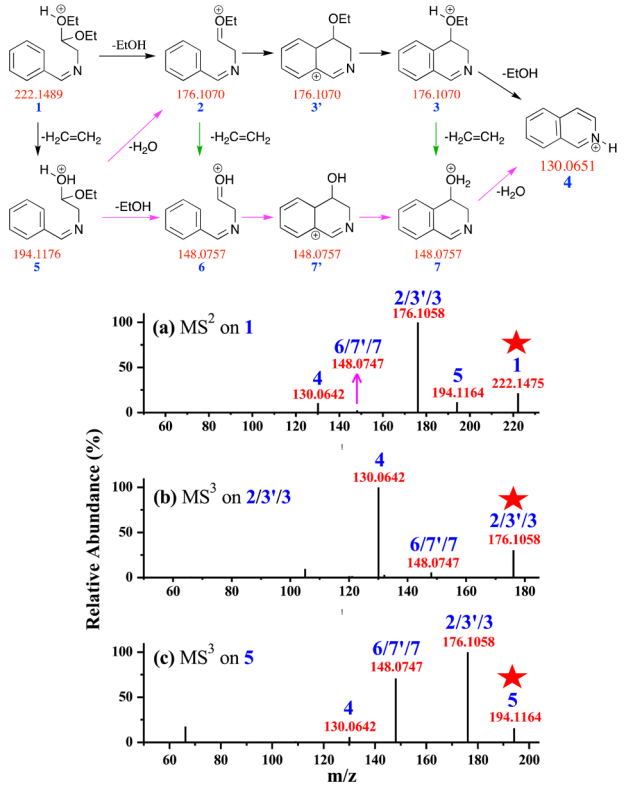

Figure 1. Gas-phase Pomeranz–Fritsch synthesis of isoquinoline on collision-induced dissociation (CID) of benzalaminoacetal **1**. The top panel presents the gas-phase synthetic route, which has been identified by tandem mass spectrometry: (a) CID-MS^2 of the precursor species **1** (m/z 222.1475); (b) CID-MS^3 of species **2**/**3**′/**3** (m/z 176.1058); and (c) CID-MS^3 of species **5** (m/z 194.1164). A red star marks the precursor species in each generation activated by CID. The theoretical m/z values (shown in red under their respective structures in the reaction scheme) agree closely with the experimentally observed m/z values shown in (a), (b), and (c). Unassigned peaks originated from the backbone fragmentation of the precursor and intermediates by CID.

Received: June 30, 2017
Published: September 26, 2017

DOI: 10.1021/jacs.7b06813
J. Am. Chem. Soc. 2017, 139, 14352–14355

the mass spectrometer by a soft ionization technique (e.g., electrospray ionization) and then allowed to collide with a gaseous target (e.g., helium) for the collision-induced dissociation (CID) to occur (see Note S1). Collisional activation evaluates the intrinsic reactivity of the isolated ions under solvent-free conditions.[4] It also allows us to access multistep proton-catalyzed reactions, which can take place in the gas phase by the "mobile proton model".[5] This multistep process can also be examined in separate steps by repeated mass selection followed by CID (MS^n).

Using tandem MS combined with theoretical calculations, we have identified 27 different reaction routes (mechanisms) for the Pomeranz–Fritsch synthesis of isoquinoline from the gaseous protonated benzalaminoacetal precursor. Although not previously detected, some of the intermediates from these gaseous reaction routes are similar to those proposed for their corresponding solution-phase reactions, thus providing evidence for their existence.

We prepared separately the benzalaminoacetal (see Supporting Information (SI)), which was then electrosprayed from a methanolic solution to produce protonated benzalaminoacetal (**1**) in the gas phase (Figure S1). On CID (Figure S2), precursor **1** was converted into different species as indicated by the ion signals observed in the corresponding MS^2 spectrum (Figure 1a). An ion signal at m/z 130.0642 suggested the formation of protonated isoquinoline (**4**) from **1** (m/z 222.1475), which was further verified by comparing the CID-MS^3 spectrum of **4** with the CID-MS^2 spectrum of the standard protonated isoquinoline (Figure S3). The base peak at m/z 176.1058 corresponds to the population of isomeric intermediate species **2** or **3′**, or **3** (not distinguishable by m/z; Figure 1), which can be reconciled with those proposed for the corresponding solution-phase reaction (Scheme S1).[1b,6] Although intermediates **2** and **3** were proposed earlier in the solution-phase Pomeranz–Fritsch synthesis of isoquinoline, they were not experimentally observed. In the present gas-phase study, we detected these isomeric species with high mass accuracy (6.8 ppm). In addition, theoretical calculations supported their formation in the gas-phase in an energetically favorable pathway (vide infra). Thus, gaseous **1** parallels the reaction behavior observed in solution.

Figure 1a also shows the formation of two other ions at m/z 194.1164 and 148.0747, corresponding to $\Delta m/z$ 28.0311 from their neighboring ions **1** and **2/3′/3**, respectively. This $\Delta m/z$ value matches well with the neutral loss of ethylene (molecular weight 28.0313) from **1** and **2/3** with high mass accuracy (7 ppm). Indeed, the loss of neutral ethylene from the oxonium ion of −OEt was detected previously by Bowen and Derrick.[7]

To determine whether ethylene can be lost from species **2/3**, we mass-selected the species (m/z 176.1058) and performed CID-MS^3. Figure 1b clearly indicates that collisional activation causes the loss of ethylene from **2/3**, resulting in the formation of species **6** from **2** and/or species **7** from **3**, as shown in the upper panel of Figure 1. An intense ion signal of protonated isoquinoline **4** is also evident in the MS^3 spectrum of **2/3′/3** (Figure 1b), indicating the transformation of **2/3′/3** into isoquinoline **4** by the neutral loss of ethanol (EtOH). When species **5** (m/z 194.1164; Figure 1a), formed by ethylene loss from **1**, was mass selected and subjected to CID-MS^3 (Figure 1c), we observed that **5** can be transformed into **2/3′/3** and **6/7′/7** to yield **4**. From the above tandem MS experiments, it is clear that **5** is the precursor of both **2/3′/3** and **6/7′/7**, and **2/3** is the precursor of **6/7**.

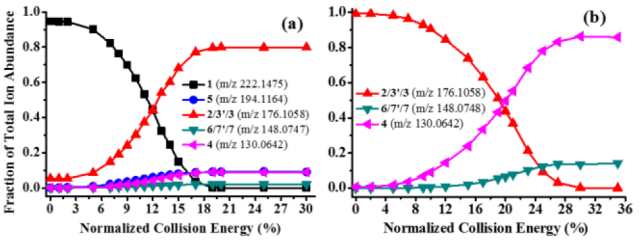

Figure 2. Breakdown curves (energy-resolved transformation profiles) of (a) **1** (m/z 222.1475), which produces species **2**–**7** in MS^2, and (b) **2** or **3** (m/z 176.1058), which produce **6** or **7**, and **4** in MS^3. Species **2** and **3**, as well as **6** and **7**, are isomeric and cannot be distinguished by their m/z values.

The top panel in Figure 1 shows the complete network discovered for the synthesis of gas-phase isoquinoline from **1** upon collisional activation. It is important to note that CID revealed this complicated reaction network due to the mobility of the attached proton in different proton receptor sites on the precursor and intermediates as attributed to the mobile proton model.[5] Some unassigned, weak ion signals in the tandem MS data (Figure 1b,c) appeared from the nonselective dissociation of the precursor **1** and intermediates **2**, **5**, and **6**. These species do not contribute to the reaction pathway shown in Figure 1.

We performed CID on **1** (MS^2; Figure 1a) and **2/3′/3** (MS^3; Figure 1b) at different collision energies and results are presented as breakdown curves in Figure 2. The fractional abundance of **4** increases with increasing normalized collision energy (NCE) and reaches a plateau at NCE ∼20% in the MS^2 of **1** (Figure 2a), and at NCE ∼30% in the MS^3 of **2/3′/3** (Figure 2b). Although the intermediates **2/3′/3** were abundant in the MS^2 of **1** (Figure 2a), the MS^3 of **2/3′/3** was enriched with the product **4** (Figure 2b).

We also conducted CID on deuterated **1** (**1D**; Figure S4), produced in the gas phase by electrospraying benzalaminoacetal from deuterated methanol (CD_3OD). Interestingly, **1D** produced both protonated as well as deuterated product ions (intermediates and products; Figure S4, top) upon collisional activation. The mobile proton model[5] once again accounts for the reaction behavior of **1D** in the gas phase, where hydrogen–deuterium (H/D) exchange occurs in the activated states of the reactant and intermediates. However, this H/D exchange process in the activated state cannot explain the formation of the species at m/z 177.1110 (Figure S4) using the reaction network proposed in Figure 1. This ion signal can be attributed to the loss of EtOH from **1D** to form the isomeric species **2′D** and/or **3′D**, which are associated with another reaction route **1D→2′D→3′D→4/4D** (Figure S4). It should be noted that the CID of the corresponding gaseous protonated species **1** could not distinguish this type of unusual reaction route from its analogous reaction route **1→2→3′→3→4** (Figure 1), although that might remain involved for the reaction of **1**. However, CID on deuterated species **1D** can clearly distinguish and anticipate this route (**1D→2′D→3′D→4/4D**; Figure S4). Indeed, many uncommon reaction routes are known to be involved in the unimolecular reaction of a collisionally excited precursor species. This is due to the proton mobility in the excited states and sequential deposition of energy under multiple collisions, which offers the possibility of many complex bond rearrangement and elimination reactions.[5b,8]

To further explore the gas-phase proton-catalyzed synthesis of the other benzopyridine, i.e., quinoline, we also performed CID on the precursors used in two classic solution-phase syntheses of

DOI: 10.1021/jacs.7b06813
J. Am. Chem. Soc. 2017, 139, 14352–14355

quinoline: the Combes quinoline synthesis[1b] and the Friedländer quinoline synthesis.[1b,9] The detailed results are described in Notes S1 and S2. Although Combes quinoline synthesis in the gas phase showed only one pathway similar to its solution-phase counterparts, Friedländer quinoline synthesis in the gas phase followed additional pathways which do not occur in solution.

Many of the species involved in the fragmentations have flexible conformational degrees of freedom. Thus, a complete understanding of the many fragmentation mechanisms must include all reaction pathways for the vast number of different conformers. Unfortunately, a comprehensive search is often prohibitive as it requires computing separate reaction pathways connecting each reactant conformer with each product conformer. In an effort to overcome this, we introduce a simplified "backtracking" scheme to compute an approximate energy profile for reaction sequences involving species with a large number of conformational degrees of freedom.

The idea of backtracking is demonstrated schematically in Figure S5. For a sequence of reactions **A**→**B**→**C**, each reaction species has several conformers, shown as pink curves in Figure S5. In this specific example, **A** and **B** both have 3 conformers (**A1**−**A3** and **B1**−**B3**) while **C** has 2 conformers (**C1**, **C2**). Backtracking analysis on **A**→**B**→**C** starts from the final product **C**. We focus on **B**→**C** pathways that generate the energetically most stable conformer **C2**, as **C2** would be the most populated conformer of **C** upon equilibration. Among these pathways, two are singled out: **B2**→**C2** with the lowest barrier, and **B1**→**C2** with the most stable reactant. In the following, we refer to these as the lowest barrier path (path-L) and the most stable reactant path (path-S), respectively. Path-L provides an estimate for the lowest **B**→**C** barrier and path-S is the barrier for a reaction which starts and ends in the most stable conformer (this would often be the only path considered if the reaction was purely statistical). For this example, path-L and path-S are the same for the **A**→**B** reaction. Once this backtracking analysis reaches the reactant, the step with the highest path-L barrier is the estimated rate-determining step (rds) for the sequence.

In addition to the usual statistical assumptions of transition-state theory, backtracking makes two critical assumptions. First, transitions between reactant conformers are assumed to be fast compared to the reactive step. Second, rates for reactive transitions ending in the most stable product conformer are assumed to be faster than (or at least similar to) rates for transitions ending in less stable product conformers. These assumptions are most likely to hold in cases where conformational transitions for the intermediates are quite facile.

We performed an extensive computational study of the reaction network for the Pomeranz−Fritsch synthesis of isoquinoline (Figure 1). For many species in the network, there exists an isomer with the proton residing on the N atom, which MS cannot distinguish from its O-protonated counterpart. Thus, in addition to the network shown in Figure 1, we also found one (Figure S6) involving N-protonated species. Additionally, we found pathways for proton transfer from O to N for several species (Figure S7), linking the two networks. For each species in the super network with flexible subgroups (**1**, **2**, **5**, and **6**), we generated at least 10 low-energy conformers (structures and energies available in SI). We classify these as *Z* and *E* according to the torsion about the C═N double bond (Figure S8).

We find that N-protonated species (**1NH**, **2NH**, **5NH**, and **6NH**), are usually more stable than their O-protonated counterparts (**1**, **2**, **5**, and **6**). For the same species (with the same protonation state), *Z* conformers are usually more stable than *E* conformers. We then did backtracking analysis for the super network (Table S1). Traversing through the super network, we found 27 different routes from the initial reactant **1** (or **1NH**) to the final product **4**, with rds listed in Table S2.

The route with the lowest barrier, **1**→**2**→**3′**→**3**→**4** (Figure 3a, Table S2), has the same mechanism as the solution-phase

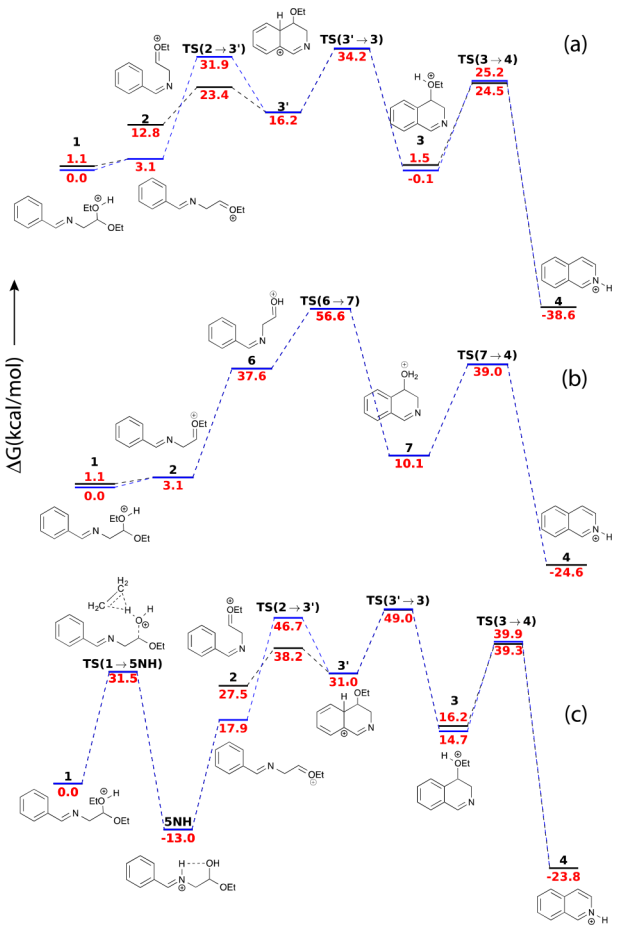

Figure 3. Energy profiles of three typical routes for the gas-phase Pomeranz−Fritsch synthesis of isoquinoline: (a) **1**→**2**→**3′**→**3**→**4**, (b) **1**→**2**→**6**→**7**→**4**, and (c) **1**→**5NH**→**2**→**3′**→**3**→**4**. Black and blue bars denote conformers participating in path-L and path-S, respectively.

Pomeranz−Fritsch synthesis (Scheme S1). Although the most stable conformer (*Z* conformer) of **2** is more stable than the path-L reactant (*E* conformer) by 10 kcal/mol, its barrier for ring closure to form **3′** is much higher (29 vs 11 kcal/mol; Figure 3a). This matches the intuition that the *Z* conformer has a more stretched structure and thus can be less readily folded to close the ring. For the subsequent proton transfer **3′**→**3**, the barrier is ∼18 kcal/mol for both path-L and path-S. Step **3**→**4** in Figure 3a determines the rds for the **1**→**2**→**3′**→**3**→**4** route and consists of the dissociation of a second EtOH along with a proton transfer. The computed barriers for path-L and path-S for this step are 23 and 25 kcal/mol, respectively. It is worth noting that there are two other competing routes, **1NH**→**2**→**3′**→**3**→**4** (Figure S9l) and **1NH**→**2NH**→**3NH**→**4** (Figure S9o), both indistinguishable from **1**→**2**→**3′**→**3**→**4** by *m*/*z*. The initial reactant, **1NH**, is more stable than **1** by 28 kcal/mol. However, the barriers for these two routes are much higher (32 and 47 kcal/mol) because

DOI: 10.1021/jacs.7b06813
J. Am. Chem. Soc. 2017, 139, 14352−14355

of proton transfer coupled dissociation (**1NH→2**), and ring closure of the N-protonated species (**2NH→3NH**).

Other routes with relatively low barriers generally form the isomeric molecules **6**/**7** (*m*/*z* 148.0747). The reactions that form these species, **2→6** and **3→7**, have barriers of 34 and 35 kcal/mol, respectively. Figure 3b shows the energy profile of the energetically most favorable route in this category: **1→2→6→7→4**. The rds **2→6** in Figure 3b has a barrier height of 34 kcal/mol, which exceeds the rds **3→4** in Figure 3a by 11 kcal/mol. The transformation **7→4** also requires 6 kcal/mol more energy than direct formation of **4** from **3**. Here we note that routes involving the formation of the two isomeric molecules, **6NH**/**7NH**, have much higher barriers due to the formation of energetically unfavorable intermediates (Figure S9, Table S2). The differences between these routes become more apparent when looking at **3NH→7NH** and **7NH→4**, which suffer from large barrier heights of 54 and 55 kcal/mol, respectively.

Routes involving the formation of **5**/**5NH** by ethylene loss from **1**/**1NH** (Figure S9) were found to have high energy barriers. For example, **1→5NH**, **1→5**, and **1NH→5NH** have increasing barriers of 31, 44, and 54 kcal/mol, respectively. Our calculations predict that the reactions **1→5** and **1NH→5NH** follow a previously proposed mechanism;[7] however, we found **1→5NH** follows a new mechanism (Movie S1) where the ethyl group first detaches from the protonated ethoxy group and then attaches to the nearby imine nitrogen, followed by its detachment again to form a transition state as shown in Figure 3c. To enable this reaction, **1** needs to be in a *Z* conformer that places the protonated ethoxy group and the imine nitrogen in close proximity. Figure 3c shows the energy profile of the energetically most favorable route in this category: **1→5NH→2→3→3′→4**. The first step (**1→5NH**) is the rds, with a barrier of 31 kcal/mol, larger than the suggested energy profiles in Figure 3a by 8 kcal/mol.

Energy profiles for 24 other mechanistic routes are provided in Figure S9. Taken together with Figure 3, these account for the complicated reaction network identified by CID of the deuterated species **1D** (Figure S4).

In summary, we have shown the syntheses of isoquinoline in the gas phase by collisional activation of the precursor protonated species, used in the classic solution-phase Pomeranz−Fritsch synthesis of isoquinoline. Proton mobility in the gaseous activated states of the precursor protonated species resulted in formation of the product isoquinoline via a number of intermediates, some of which cannot be formed in solution. Tandem mass spectrometry along with isotope labeling identified these intermediates and products, which assisted in revealing the routes responsible for gas-phase synthesis of isoquinoline. In addition, it was shown that some of these routes differ significantly from their condensed-phase counterparts. Unlike the corresponding solution-phase reactions (where the reaction conditions are thermalized and catalytic proton exchange occurs between intermediates and solvent (Brønsted−Lowry base)), these gas-phase reactions occur under collisionally excited conditions. Here, energy is deposited in the protonated molecule by multiple collisions with the inert gas (helium) in the ion trap and proton hopping causes new intermediates to appear. Thus, the difference in reactivity in the condensed phase and in the gas phase is quite evident. Nevertheless, we showed that products resulting from gas-phase and solution-phase synthesis of isoquinoline are identical, but the particular paths to such products can be very different.

■ ASSOCIATED CONTENT

Supporting Information

The Supporting Information is available free of charge on the ACS Publications website at DOI: 10.1021/jacs.7b06813.

Experimental and computational details, Notes S1−S3, Schemes S1−S3, Figures S1−S22, and Tables S1−S4 (PDF)

Movie S1 (MPG)

■ AUTHOR INFORMATION

Corresponding Author

*zare@stanford.edu

ORCID

Shibdas Banerjee: 0000-0002-3424-8157

Fang Liu: 0000-0003-1322-4997

Todd J. Martínez: 0000-0002-4798-8947

Richard N. Zare: 0000-0001-5266-4253

Author Contributions

#S.B. and F.L. contributed equally.

Notes

The authors declare no competing financial interest.

■ ACKNOWLEDGMENTS

This work was supported by the Air Force Office of Scientific Research through Basic Research Initiative grant (AFOSR FA9550-16-1-0113), National Science Foundation under the CCI Center for Selective C−H Functionalization (CHE-1205646), and Office of Naval Research (N00014-14-1-0590). D.M.S. is grateful to the NSF for a graduate fellowship.

■ REFERENCES

(1) (a) Gensler, W. J. *Organic Reactions*; Wiley: New York, 2004. (b) Li, J. J. *Name Reactions: A Collection of Detailed Mechanisms and Synthetic Applications*, 5th ed.; Springer: Switzerland, 2014.

(2) (a) Birch, A. J.; Jackson, A. H.; Shannon, P. V. R. *J. Chem. Soc., Perkin Trans. 1* **1974**, 2185. (b) Wang, Z. *Comprehensive Organic Name Reactions and Reagents*; Wiley: Hoboken, NJ, 2010.

(3) Banerjee, S.; Zare, R. N. *Angew. Chem., Int. Ed.* **2015**, *54*, 14795.

(4) (a) McLafferty, F. *Science* **1981**, *214*, 280. (b) Fisher, E. R.; Kickel, B. L.; Armentrout, P. B. *J. Phys. Chem.* **1993**, *97*, 10204. (c) Mitchell Wells, J.; McLuckey, S. A. *Methods in Enzymology*; Academic Press: Cambridge, 2005; Vol. *402*, p 148. (d) Cheng, C.; Gross, M. L. *Mass Spectrom. Rev.* **2000**, *19*, 398. (e) Wang, H.-Y.; Zhang, X.; Guo, Y.-L.; Tang, Q.-H.; Lu, L. *J. Am. Soc. Mass Spectrom.* **2006**, *17*, 253. (f) Pruesse, T.; Fiedler, A.; Schwarz, H. *J. Am. Chem. Soc.* **1991**, *113*, 8335. (g) Glish, G. L.; Cooks, R. G. *J. Am. Chem. Soc.* **1978**, *100*, 6720.

(5) (a) Dongré, A. R.; Jones, J. L.; Somogyi, Á.; Wysocki, V. H. *J. Am. Chem. Soc.* **1996**, *118*, 8365. (b) Banerjee, S.; Mazumdar, S. *J. Am. Soc. Mass Spectrom.* **2012**, *23*, 1967.

(6) Bobbitt, J. M.; Bourque, A. J. *Heterocycles* **1987**, *25*, 601.

(7) Bowen, R. D.; Derrick, P. J. *J. Chem. Soc., Chem. Commun.* **1990**, 1539.

(8) (a) Harrison, A. G.; Young, A. B.; Bleiholder, C.; Suhai, S.; Paizs, B. *J. Am. Chem. Soc.* **2006**, *128*, 10364. (b) Bythell, B. J.; Maître, P.; Paizs, B. *J. Am. Chem. Soc.* **2010**, *132*, 14766.

(9) Cheng, C.-C.; Yan, S.-J. *Organic Reactions*; Wiley: New York, 2004.

DOI: 10.1021/jacs.7b06813
J. Am. Chem. Soc. 2017, 139, 14352−14355